PNAS
www.pnas.org

Supplementary Information Appendix for

Inhibition Mechanisms of AcrF9, AcrF8, and AcrF6 Against Type I-F CRISPR-Cas Complex Revealed by Cryo-EM

Kaiming Zhang[1,#], Shuo Wang[2,#], Shanshan Li[1,#], Yuwei Zhu[2,#], Grigore Pintilie[1], Tung-Chung Mou[3], Michael F. Schmid[4], Zhiwei Huang[2,*], Wah Chiu[1,4,*]

[1]Departments of Bioengineering, and of Microbiology and Immunology, and James H. Clark Center, Stanford University, Stanford, CA 94305 USA
[2]HIT Center for Life Sciences, School of Life Science and Technology, Harbin Institute of Technology, Harbin 150080, China
[3]Center for Biomolecular Structure and Dynamics, University of Montana, Missoula, MT 59812, USA
[4]CryoEM and Bioimaging Division, SSRL, SLAC National Accelerator Laboratory, Stanford University, Menlo Park, CA 94025 USA

*Correspondence: huangzhiwei@hit.edu.cn (Z.H.), wahc@stanford.edu (W.C.)
[#]These authors contributed equally to this work

www.pnas.org/cgi/doi/10.1073/pnas.1922638117

This PDF file includes:

Figs. S1 to S12
Tables S1 to S2
Movie S1

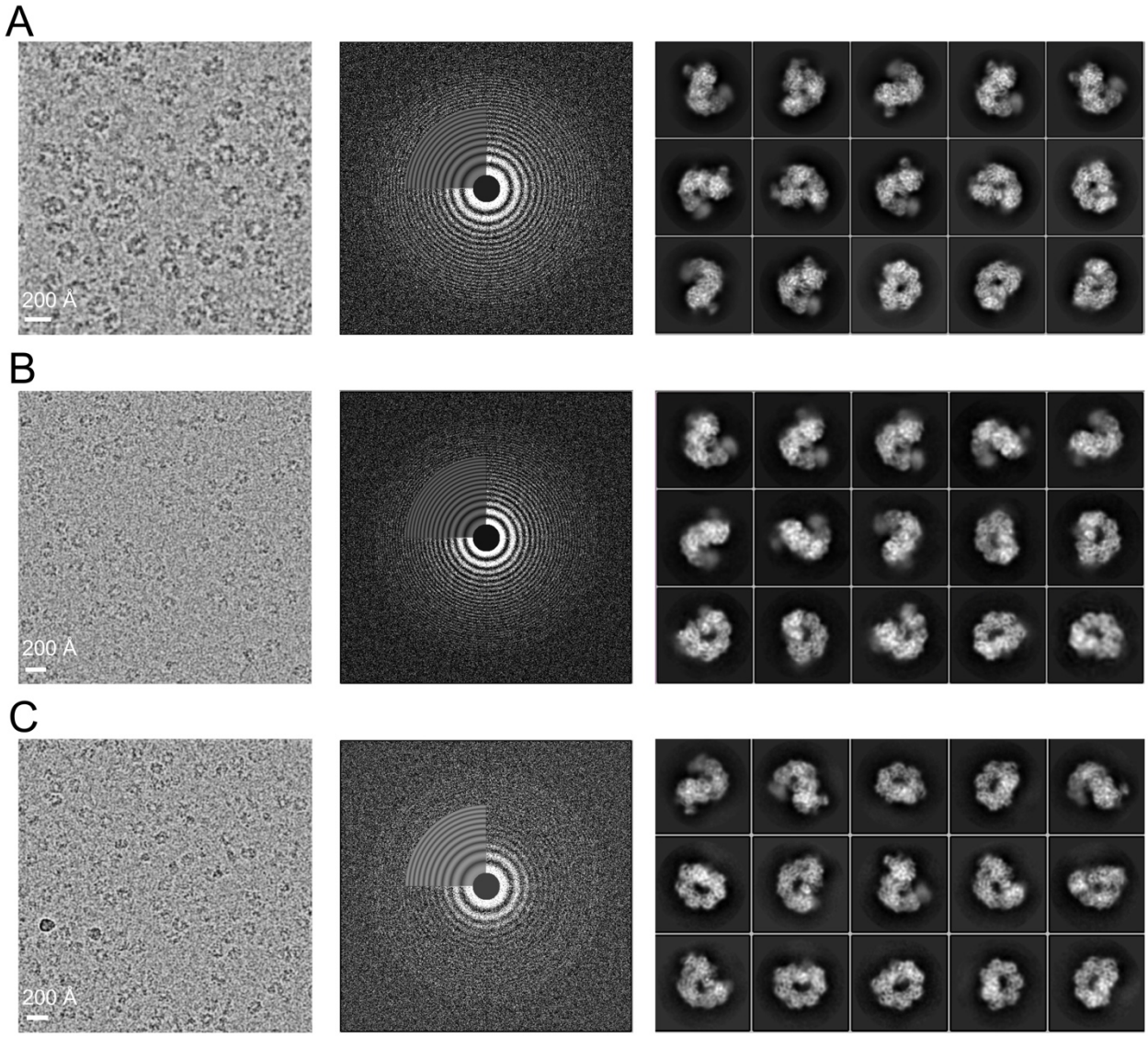

Fig. S1. Cryo-EM raw data and 2D analysis. (*A*) Csy-AcrF9 complex. Left: representative motion-corrected cryo-EM micrograph; middle: representative Fourier transform with Thon rings extending to 1.98 Å calculated by CTFFIND4; right: reference-free 2D class averages. (*B*) Csy-AcrF8 complex. Left: representative motion-corrected cryo-EM micrograph; middle: representative Fourier transform with Thon rings extending to 2.31 Å calculated by CTFFIND4; right: reference-free 2D class averages. (*C*) Csy-AcrF6 complex. Left: representative motion-corrected cryo-EM micrograph; middle: representative Fourier transform with Thon rings extending to 2.87 Å calculated by CTFFIND4; right: reference-free 2D class averages.

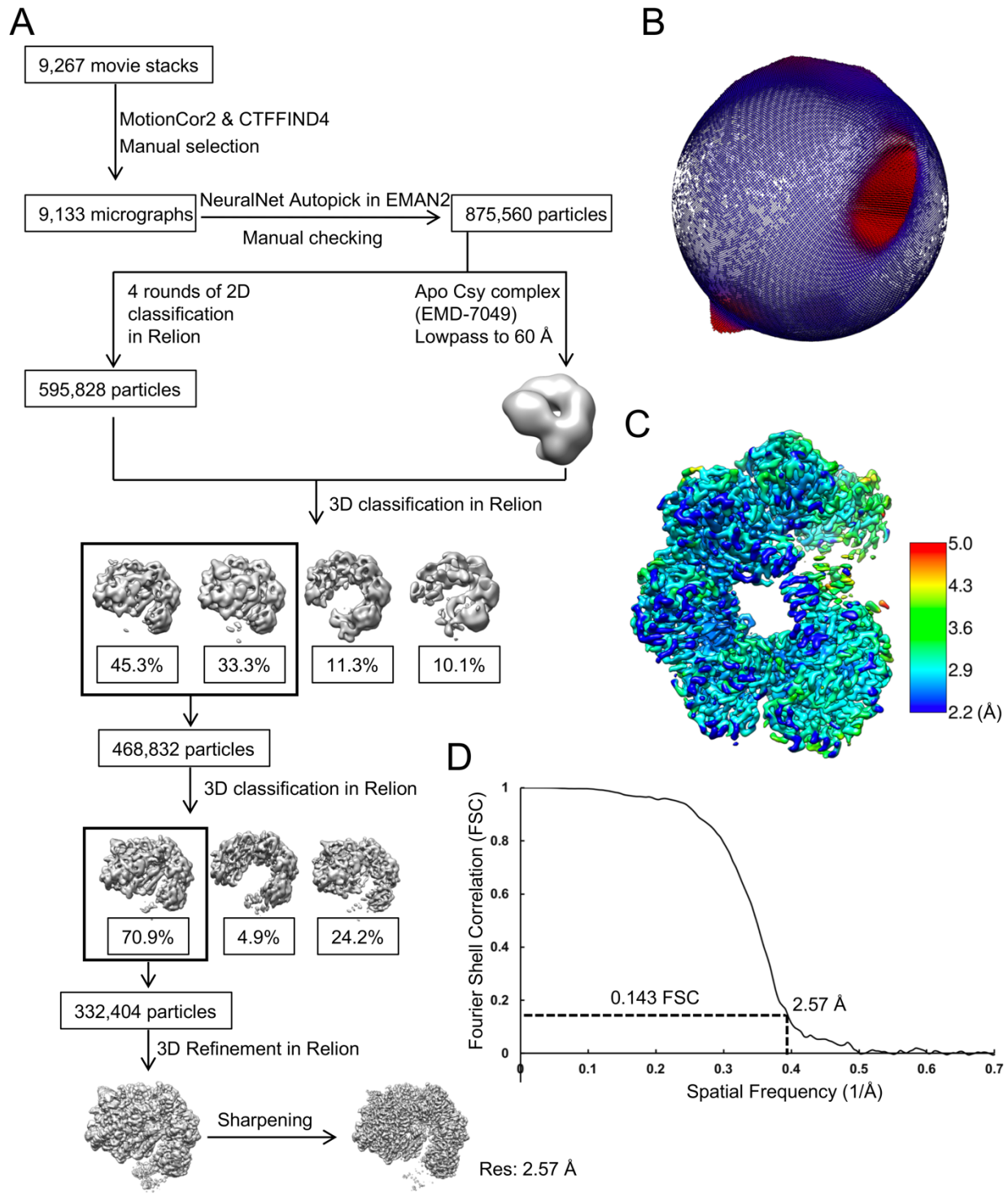

Fig. S2. Single-particle cryo-EM analysis of the Csy-AcrF9 complex. (*A*) Workflow of cryo-EM data processing. (*B*) Euler angle distribution of all particles used for calculating the final 3D reconstruction. (*C*) Resolution map for the final 3D reconstruction. (*D*) Gold standard FSC plot for the final 3D reconstruction.

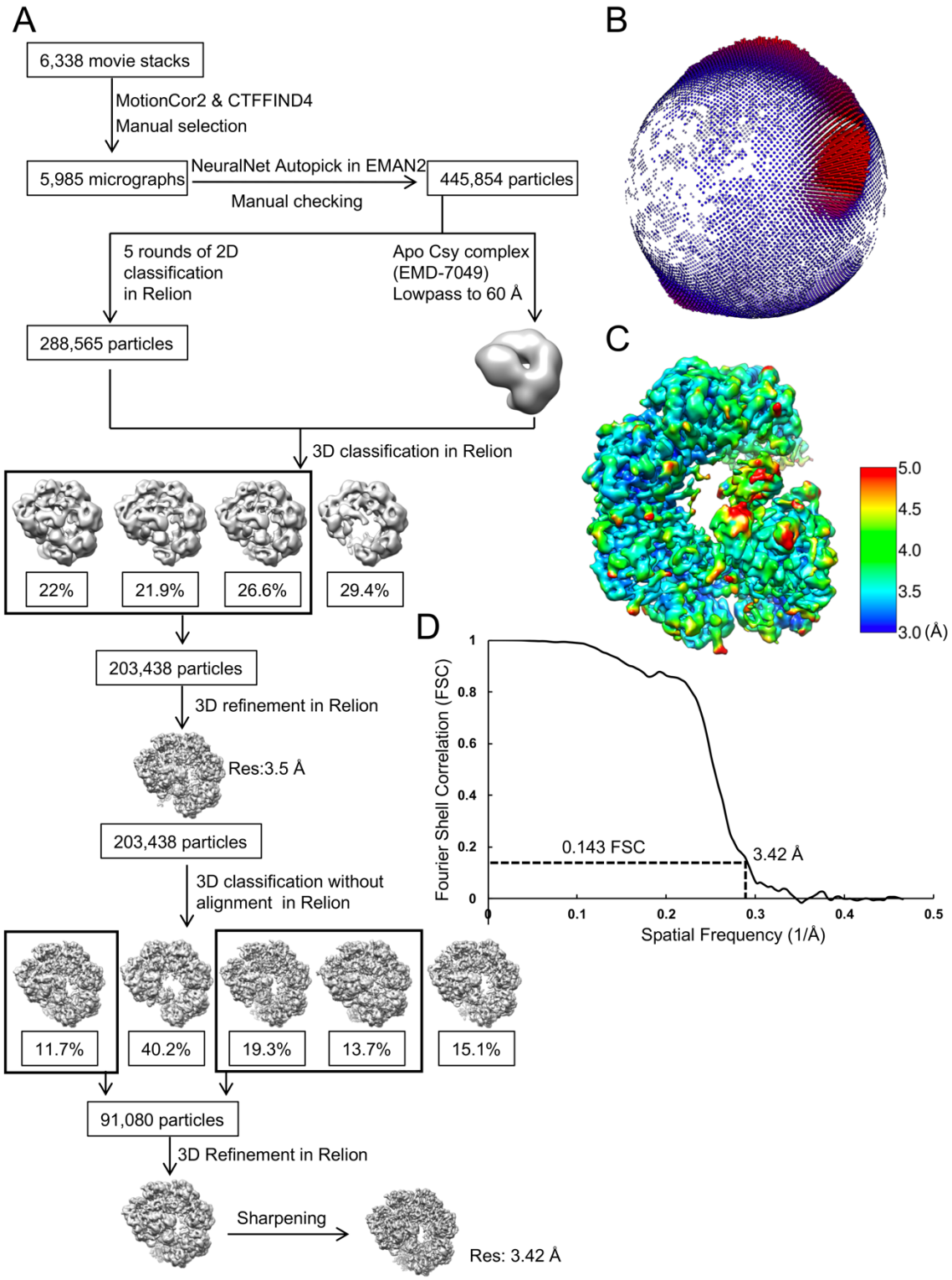

Fig. S3. Single-particle cryo-EM analysis of the Csy-AcrF8 complex. (*A*) Workflow of cryo-EM data processing. (*B*) Euler angle distribution of all particles used for calculating the final 3D reconstruction. (*C*) Resolution map for the final 3D reconstruction. (*D*) Gold standard FSC plot for the final 3D reconstruction.

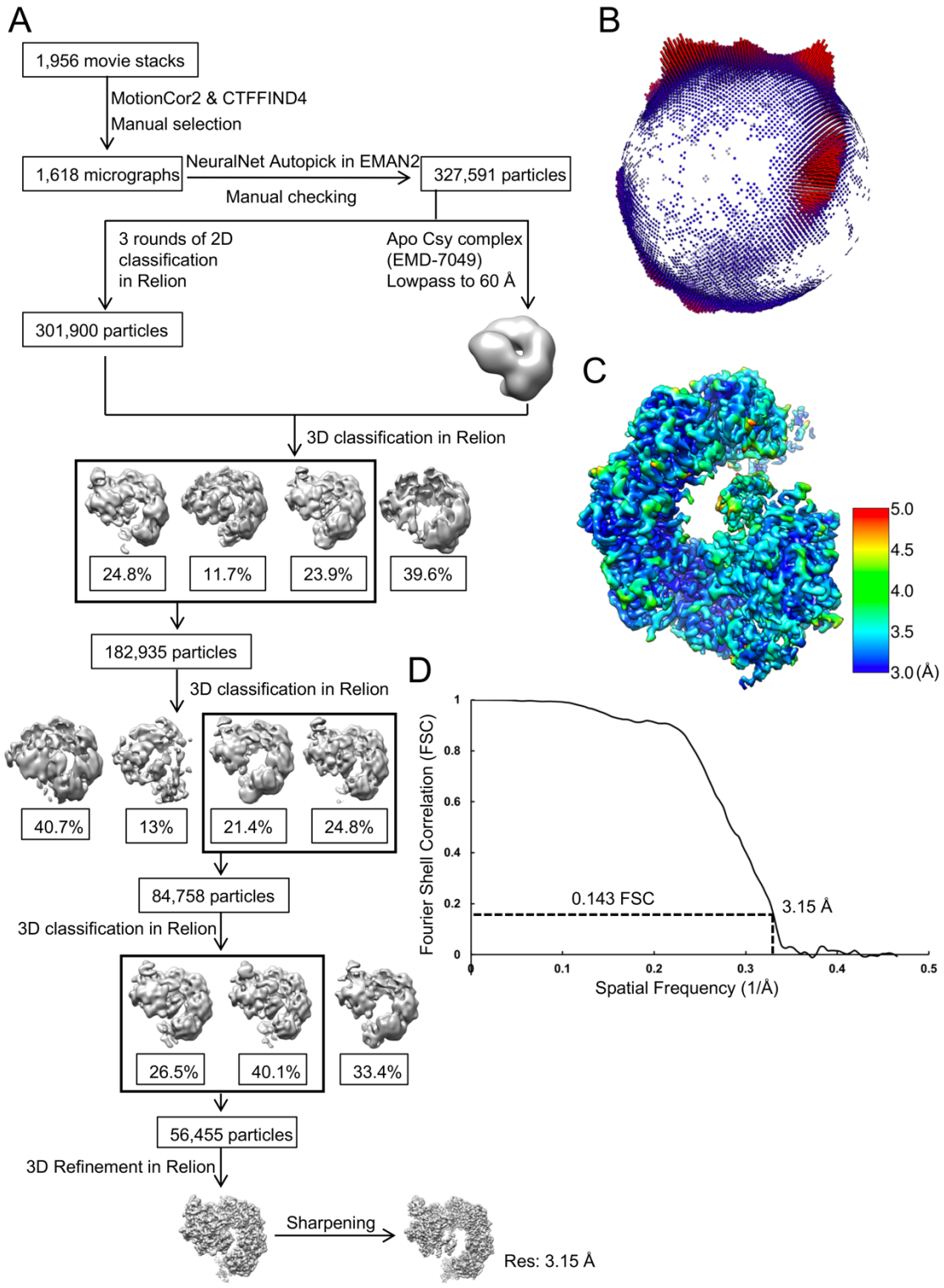

Fig. S4. Single-particle cryo-EM analysis of the Csy-AcrF6 complex. (*A*) Workflow of cryo-EM data processing. (*B*) Euler angle distribution of all particles used for calculating the final 3D reconstruction. (*C*) Resolution map for the final 3D reconstruction. (*D*) Gold standard FSC plot for the final 3D reconstruction.

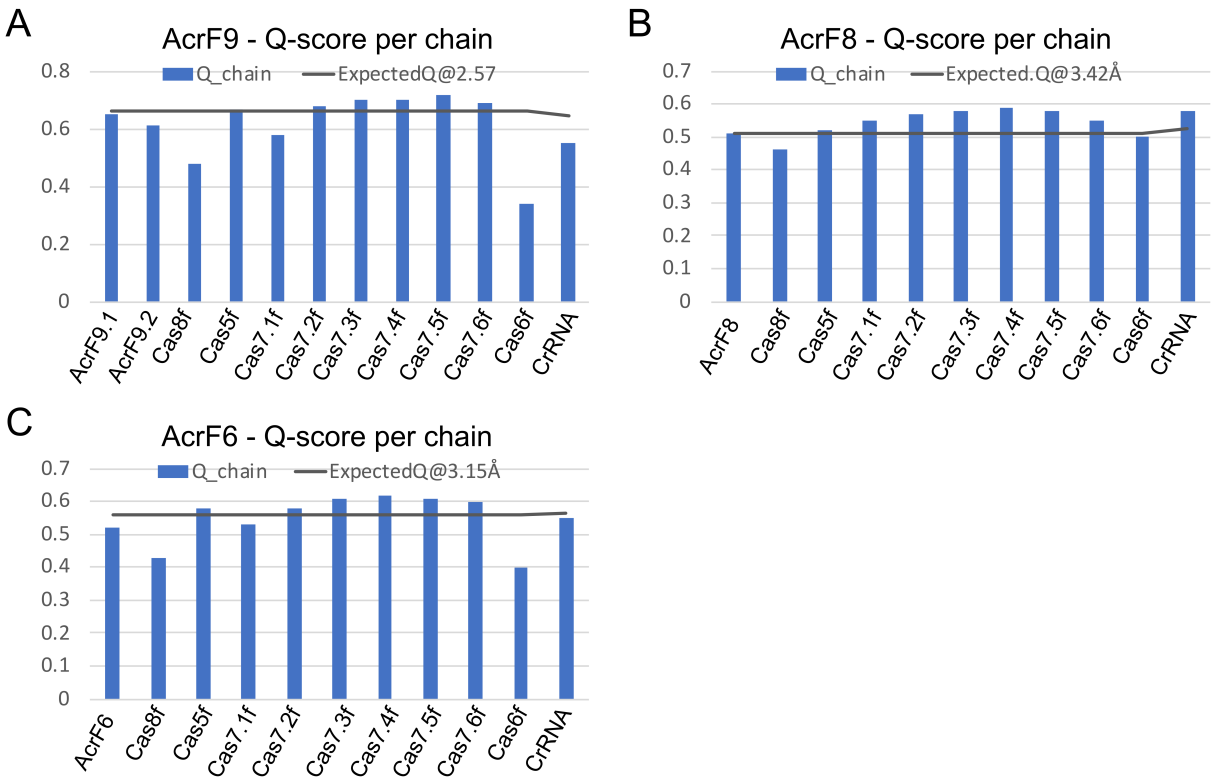

Fig. S5. Resolvability of the cryo-EM structures of Csy-AcrF9 (*A*), Csy-AcrF8 (*B*), and Csy-AcrF6 (*C*) complexes calculated by Q-score. Q-score for each chain in models and maps of the three complexes; the black line represents the expected Q-score at respective resolution based on the correlation between Q-scores and map resolution of proteins and RNAs. The higher Q-score indicates better resolvability.

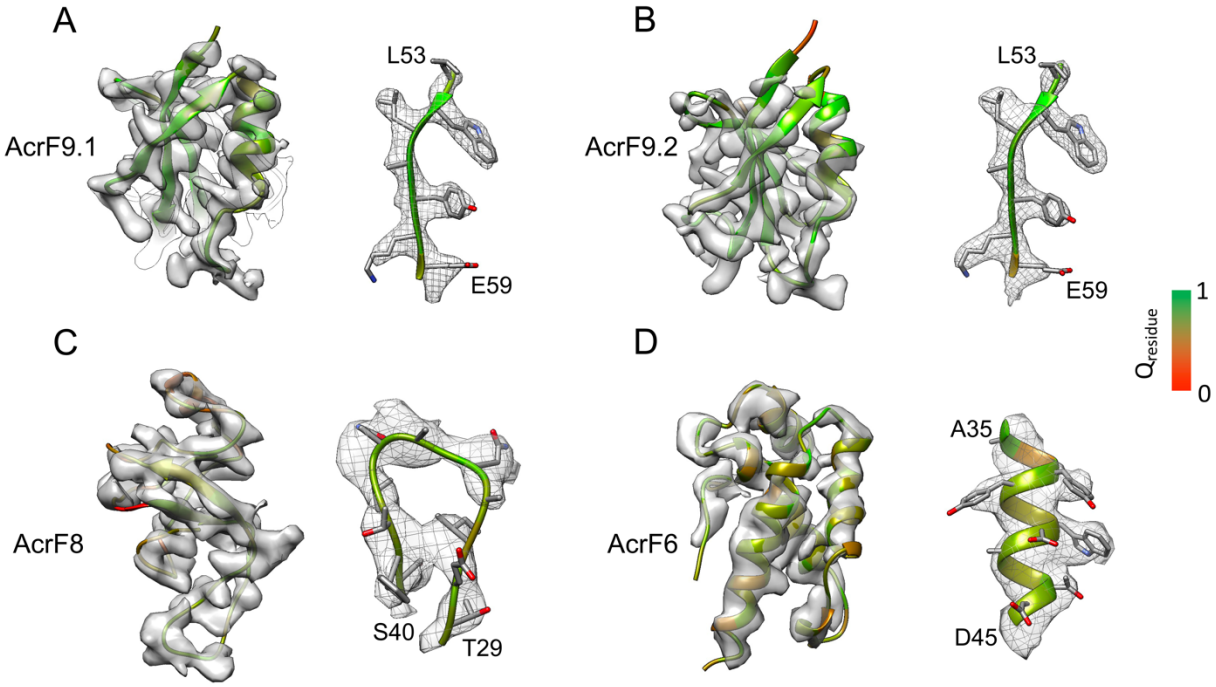

Fig. S6. Resolvability of the cryo-EM structures of AcrF9 (*A, B*), AcrF8 (*C*), and AcrF6 (*D*) calculated by Q-score. The model is shown as ribbon, with Q-scores colored. The higher Q-score indicates better resolvability. A sample density is shown on the right side.

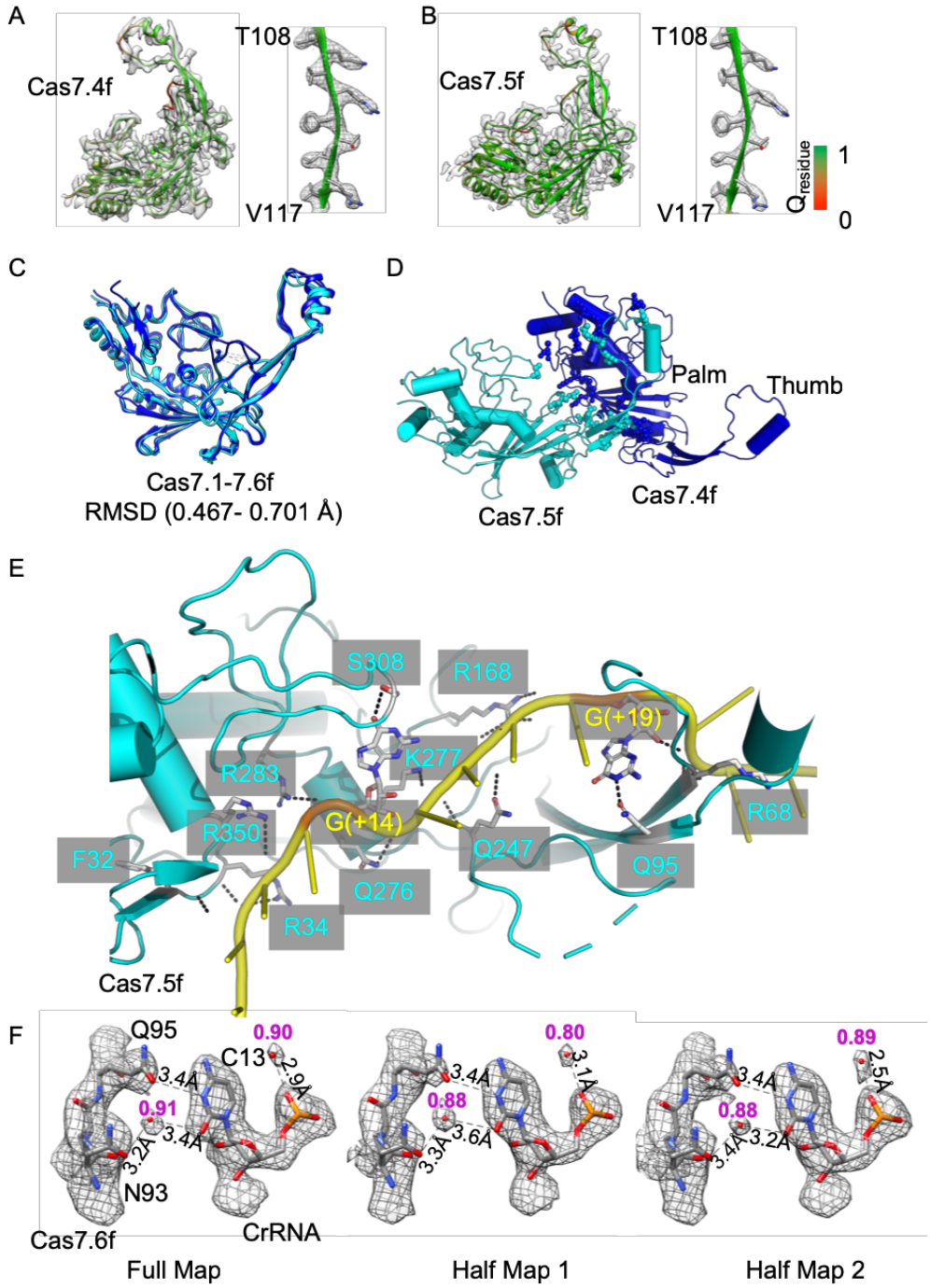

Fig. S7. Interfaces of Cas7f-Cas7f and Cas7f-crRNA. (*A, B*) Resolvability of the cryo-EM structures of Cas7.4f (*A*) and Cas7.5f (*B*) calculated by Q-score. The model is shown as ribbon, with Q-scores colored. The higher Q-score indicates better resolvability. A sample density is shown on the right side. (*C*) Superimposition of six Cas7f subunits, with the RMSD calculated. (*D*) The interface between Cas7.4f and Cas7.5f. The residues involved in the interface are listed in Table S2. (*E*) Hydrogen bonds between Cas7.5f and crRNA are shown in black dash lines. (*F*) The direct and water-mediated interactions between Cas7f proteins and crRNA. Q-scores of the waters between the map and model are calculated and shown in magenta.

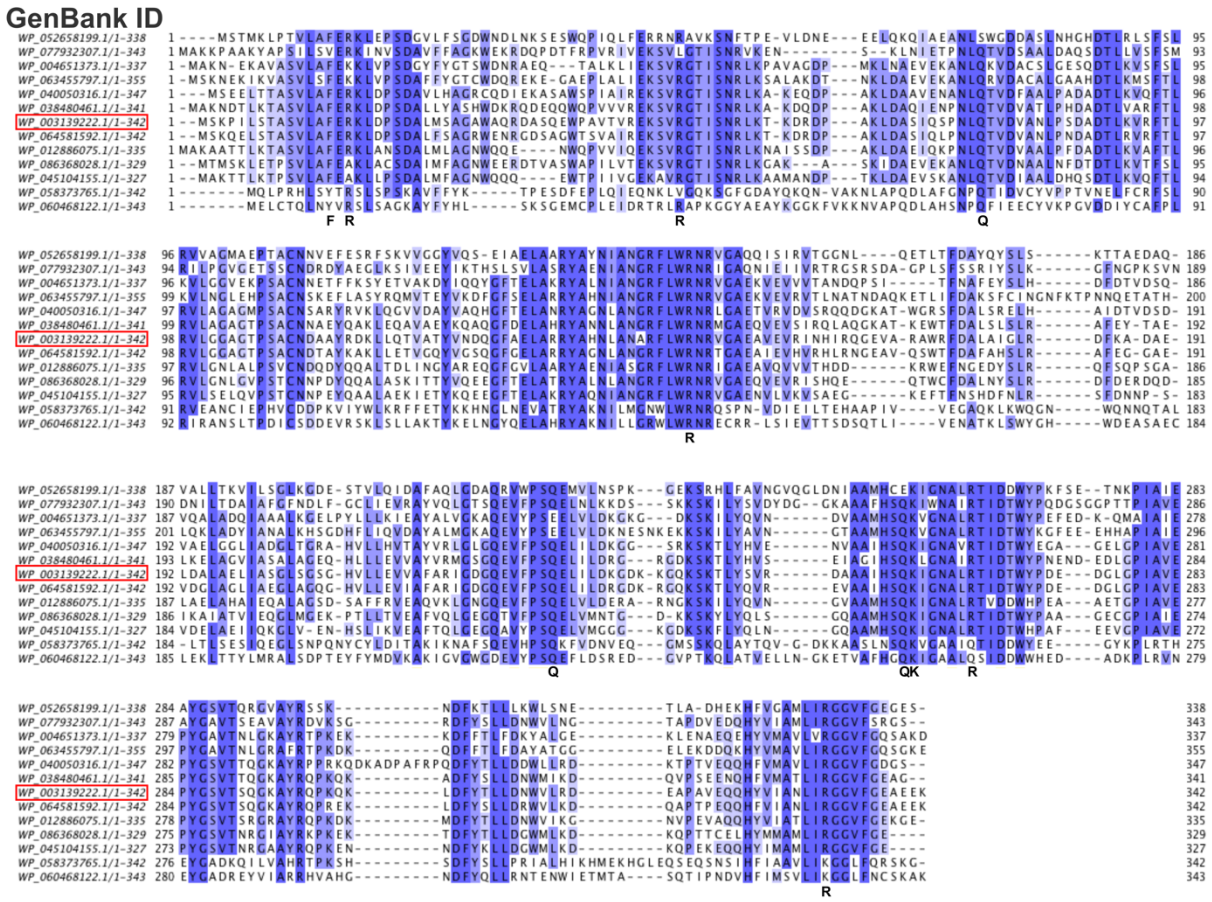

Fig. S8. Sequence alignment of Cas7f proteins from different species. *P. aeruginosa* used in our study is shown within red box. The residues are colored by % identity. Residues of Cas7f involved in crRNA binding are shown at bottom.

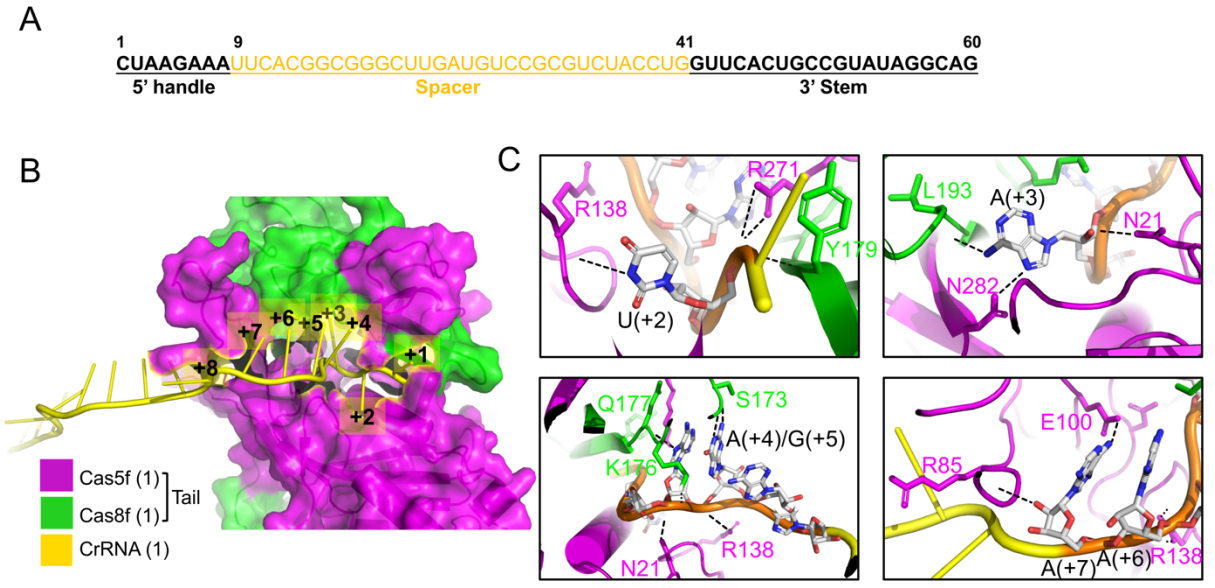

Fig. S9. Interaction analysis of the crRNA 5' handle and Cas5f-Cas8f. (*A*) Sequence of crRNA. (*B*) The interface between the crRNA 5' handle and Cas5f-Cas8f, where Cas5f and Cas8f are shown in surface representation. (*C*) Hydrogen bonds between Cas5f-Cas8f and crRNA (+2→+7) are shown in black dash lines.

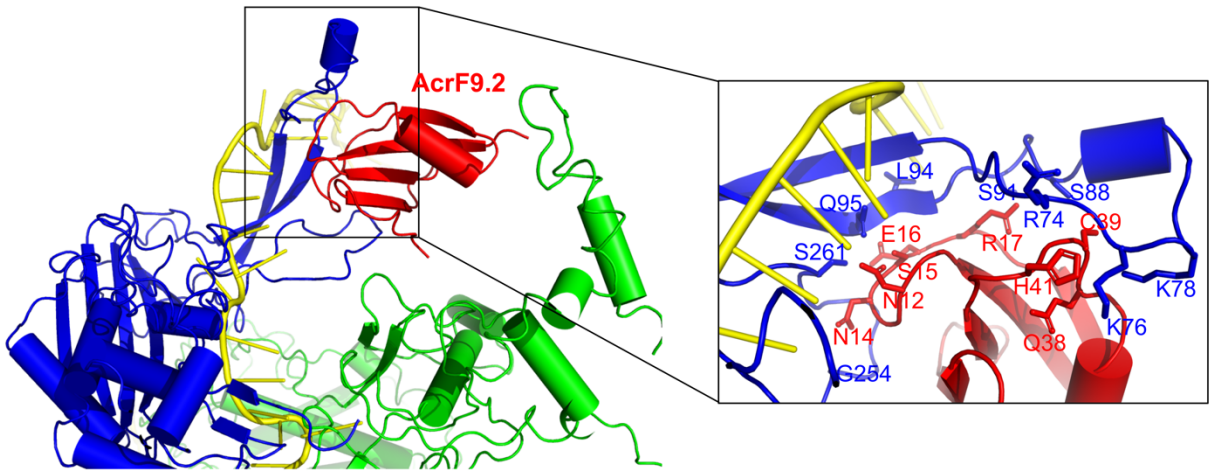

Fig. S10. Interface between AcrF9.2 and Cas7.6f. The residues involved in the interface are shown.

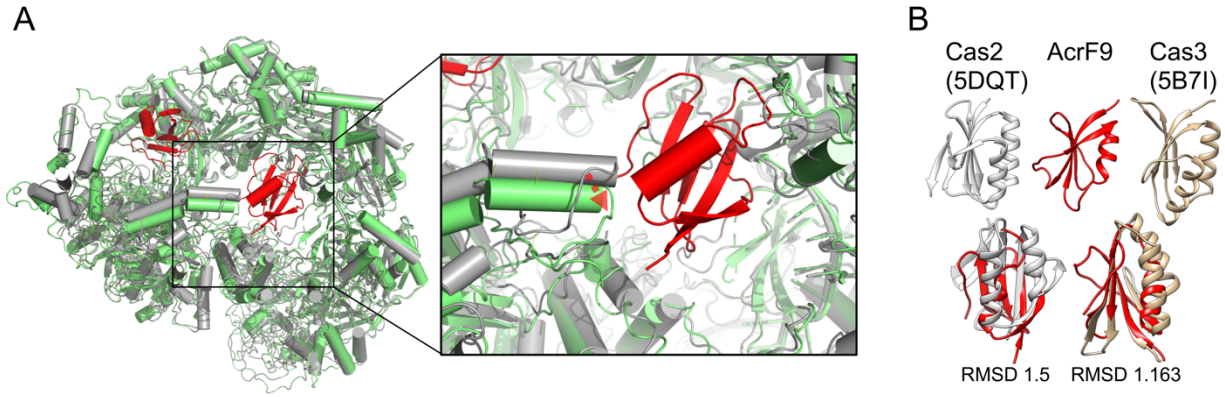

Fig. S11. Conformational change induced by the binding of AcrF9.1 (*A*) and superimposition of AcrF9 with Cas2/3 (*B*).

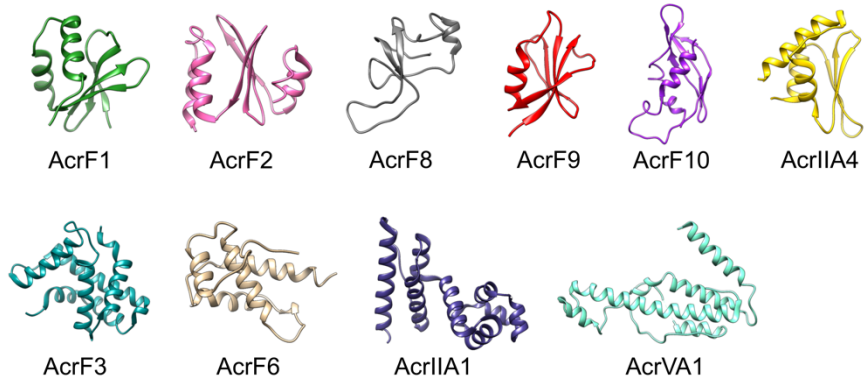

Name	PDB code	Chain
AcrF1	6B46	I
AcrF2	6B47	K
AcrF8	This work	A
AcrF9	This work	A
AcrF10	6B48	K
AcrIIA4	5VW1	B
AcrF3	5GNF	A
AcrF6	This work	A
AcrIIA1	5Y6A	A
AcrVA1	6NMD	B

Fig. S12. Ribbon representation of different Acr proteins.

Table S1. Cryo-EM data collection, processing, and model validation

	Csy-AcrF9	Csy-AcrF8	Csy-AcrF6
Data collection and processing			
Microscope	Titan Krios	Titan Krios	Titan Krios
Voltage (kV)	300	300	300
Camera	Gatan K2 Summit	Gatan K2 Summit	Gatan K2 Summit
Pixel size (Å)	0.65	1.06	1.06
Total Dose (e-/Å^2)	56	42	42
Exposure time (s)	6	6	6
Number of frames per exposure	30	30	30
Defocus range during data collection (μm)	-0.6 - -2.7	-0.6 - -3.6	-0.9 - -2.4
Number of micrographs	9,267	6,338	1,956
Number of initial particles	875,560	445,854	327,591
Number of particles for 3D analyses	595,828	288,565	301,900
Symmetry	C1	C1	C1
Number of final particles	332,404	91,080	56,455
Defocus range after data processing (μm)	-0.3 - -3.1	-0.5 - -3.7	-1.1 - -2.5
Resolution (0.143 FSC, Å)	2.57	3.42	3.15
Atomic model refinement			
Software	phenix.real_space_refine	phenix.real_space_refine	phenix.real_space_refine
Clashscore, all atoms	5.11	7.83	6.61
Protein geometry			
Poor rotamers (%)	1.16	0.57	0.04
Favored rotamers (%)	95.45	84.51	98.07
Ramachandran outliers (%)	0.07	0	0.03
Ramachandran favored (%)	91.31	86.93	91.24
MolProbity score	1.83	2.05	1.88
Bad bonds (%)	0.06	0.01	0
Bad angles (%)	0.11	0.01	0.04
Nucleic acid geometry			
Probably wrong sugar puckers (%)	1.67	0	0
Bad bonds (%)	0	0	0
Bad angles (%)	0	0	0

Table S2. The residues involved in the formation of hydrogen bonds and salt bridges between Cas7.4f and Cas7.5f subunits of the Csy complex

Hydrogen bonds	Cas7.4f			Cas7.5f		
	Atom	Res	Res no.	Atom	Res	Res no.
	NH2	ARG	34	OE1	GLU	242
	OD2	ASP	40	NH2	ARG	63
	NH1	ARG	112	O	SER	104
	O	THR	114	NE2	GLN	241
	OG1	THR	114	O	ASP	239
	OG1	THR	114	NE2	GLN	241
	NH1	ARG	116	O	GLY	172
	N	CYS	127	O	SER	308
	OE1	GLU	248	OG	SER	66
	OE2	GLU	248	N	SER	66
	N	LEU	249	OG	SER	66
	OH	TYR	265	NH1	ARG	63
	OE1	GLN	276	NZ	LYS	65
	NE2	GLN	276	O	SER	66
	NZ	LYS	317	OD1	ASP	81
	OH	TYR	323	O	SER	72
Salt bridges	OE2	GLU	33	NE	ARG	168
	NH2	ARG	34	OE1	GLU	242
	OD2	ASP	40	NH2	ARG	63
	NH2	ARG	112	OD2	ASP	239
	NZ	LYS	317	OD1	ASP	81
	OD2	ASP	327	NH1	ARG	74
	OE2	GLU	356	NE	ARG	74

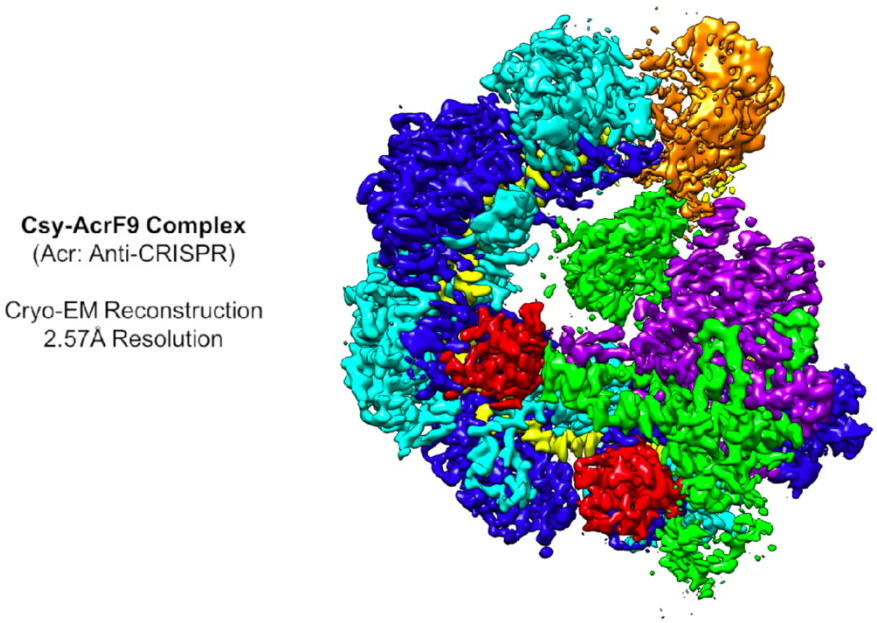

Movie S1. Overall structure (map and model) of the Type I-F CRISPR-Csy complex bound with two copies of AcrF9.